Nuclear stopping power at high energies

S. Daté, M. Gyulassy,* and H. Sumiyoshi
Institute of Nuclear Study, University of Tokyo, Tanashi, Tokyo 188, Japan
(Received 29 March 1985)

Recent $p+A \to p+X$ data are analyzed within the context of the multichain and additive quark models. We deduce the average energy loss of a baryon as a function of distance traversed in nuclear matter. Consistency of the multichain model is checked by comparing the predictions for $p+A \to \pi^{\pm}+X$ with data. We discuss the space-time development of baryon stopping and show how longitudinal growth limits the energy deposition per unit length. Predictions are made for the proton spectra to be measured in nucleus-nucleus collisions at CERN and BNL. Finally, we conclude that the stopping domain for central collisions of heavy ions extends up to center-of-mass kinetic energies $E_{\text{c.m.}} \approx (3\pm1)A$ GeV.

I. INTRODUCTION

Initial interest in hadron-nucleus collisions focused on the space-time development of multiparticle production.[1] The main role of the nucleus was to act simply as a microscopic detector sensitive to distance scales $\lesssim 10$ fm. The most important qualitative feature that emerged from those studies is the validity of the formation-zone concept.[2–4] That concept follows from time dilation and the uncertainty principle and states that the formation of a secondary particle with rapidity y and transverse mass $m_\perp$ cannot be localized within a distance $l(y,p_\perp) \approx e^y/m_\perp$ of the interaction point. This exponential growth of length scales is also referred to as longitudinal growth and explains why naive intranuclear-cascade models[5] systematically overpredict the charged-particle multiplicities[6] in proton-nucleus reactions at high energies.

Renewed interest in hadron-nucleus reactions has been stimulated by new data[7] on $p+A \to p+X$ at 100 GeV. In addition to providing new tests for competing multiparticle production models,[8–15] these data may have important consequences for quark-gluon-plasma (QGP) production in nucleus-nucleus collisions.[16] In particular, the first analysis[17] of that data indicated that the stopping power of a nucleus could be much greater than first expected. This may imply that energy and baryon densities much higher than previously thought[18] could be achieved in central nuclear collisions. Understanding nuclear stopping power is therefore essential in assessing whether high-baryon-density QGP could be produced in nuclear collisions in the energy range 10—100 GeV per nucleon (A GeV). Since that pioneering paper[17] several other works[19–22] have addressed the nuclear stopping problem. In this paper we apply the multichain model[9] and the additive quark model[13–15] to gain further insight into this problem.

The primary aim of this paper is to deduce the stopping power of nuclear matter to high-energy protons. We evaluate several quantitative measures of that stopping power. One is the average energy fraction the leading proton retains after traversing a thickness z of nuclear matter. Another measure is the average rapidity loss of a baryon, $\langle \Delta y \rangle_z$, as a function of nuclear thickness. In contrast to previous works, we can test the consistency of our methods by comparing our calculations for $p+A \to \pi^{\pm}+X$ as well as $p+A \to p+X$ with the data. Furthermore, our method treats pp reactions on the same footing as pA and AB reactions. A fit to the available data determines the one physical parameter, $\alpha = 3\pm1$, of our model that controls the inelasticity in multiple collisions. In the terminology of Ref. 20 this parameter implies a momentum-degradation length $\Lambda_p = 8\pm2$ fm at 100 GeV.

The second aim of this paper is to clarify the space-time development of the stopping process. In particular, we find that longitudinal growth limits the energy deposition per unit length and is the main factor, not the stopping power, that determines the boundaries of the stopping domain for nuclear collisions. We show that the length scales associated with secondary-particle production and baryon stopping need not coincide. We find that baryon stopping and secondary-particle production can occur within a Lorentz-contracted nuclear volume in the c.m. frame only up to center-of-mass kinetic energies $\sim(3\pm1)A$ GeV. However, by that energy, baryon and energy densities in excess of one order of magnitude above their ground-state values can be achieved in central collisions of heavy nuclei. Therefore, production of baryon-rich quark-gluon plasmas with nuclear collisions at relatively low energies is consistent with our stopping power analysis.

The organization of this paper is as follows: In Sec. II the assumptions, physical picture, and equations that define the multichain model are reviewed. In Sec. III we apply the model to fit the $pA \to \pi^{\pm}$ and $pA \to p$ data.[7] Thereby we determine the one physical parameter of the model. In Sec. IV we analyze the space-time development of stopping and estimate the boundary of the stopping domain for nuclear collisions. In Sec. V, we predict the leading-proton rapidity density for nuclear collisions that may eventually be measured[16] at CERN and BNL. In Sec. VI, an independent determination of nuclear stopping power obtained from fitting the data with the additive quark model gives additional confidence in the extrapolat-

ed stopping power to nuclear depths on the order of 14 fm. Concluding remarks are then presented in Sec. VI.

II. THE MULTICHAIN MODEL

A. Assumptions

There is much uncertainty about the low-transverse-momentum processes that lead to multiparticle production in high-energy hadron-nucleus collisions. That uncertainty obviously is deeply rooted in the unsolved nonperturbative problems associated with large distance scales in QCD. It is therefore not surprising that there exists such a large number of phenomenological models in the literature. The main virtue of the present model[9] is that is cleanly separates geometrical effects from dynamical ones, and the dynamics is characterized by one physical parameter. Since geometrical effects are separated, this model treats hadron-hadron, hadron-nucleus collisions on the same footing. Furthermore, it provides a convenient extrapolation tool to predict nucleus-nucleus reactions.

The simplifying assumptions of the multichain model are as follows.

(1) The transverse-momentum distribution is independent of incident energy, nuclear size, and longitudinal momentum.

(2) The probability that a hadron undergoes exactly n interactions is given by Glauber theory.

(3) The reaction involves two stages that determine the longitudinal-momentum distributions of the particles: a fast multiple-interaction stage and a time-dilated fragmentation stage leading to secondary-hadron production.

(4) The fragmentation stage is independent of the number of interactions involved in the first stage.

(5) The multiple-collision dynamics scales with energy. In particular, the longitudinal-momentum distribution depends only on the scaling light-cone variable

$$x=\frac{(E+p_z)}{(E+p_z)_{\max}}=e^{y-y_{\max}}, \tag{2.1}$$

where

$$y_{\max}=y_0+\ln(m_N/m_\perp)$$

is the maximum rapidity that a particle with transverse mass

$$m_\perp=(m^2+p_\perp{}^2)^{1/2}$$

can have.

(6) Projectile and target fragmentation processes are independent.

The above assumptions are surely too strong but are consistent with present phenomenology[8–17,19–22] and considerably simplify the formalism.

A physical picture consistent with the above assumptions can be formulated in terms of partons and color strings. The incoming proton is regarded as a composite object with many partons sharing the incident momentum. As that proton passes through a target nucleon one of its partons may change color due to an interaction with a parton of the target. The color exchange can be viewed as a string flip whereby the color string connecting the target parton to the spectator target partons and the string connecting the projectile parton to the spectator projectile partons interchange so that the spectator target partons now connect to the projectile parton and the spectator projectile partons now connect to the target parton. In this picture an interaction creates two strings which stretch with time.[11,23] We refer to the string connecting the spectator target partons with the interacting projectile parton as a target chain.

In proton-nucleus collisions, we regard the nucleus as a parton filter that sifts out a certain number of partons from the projectile. That sifting occurs by promoting virtual partons to their mass shell and creating independent target chains. Because of time dilation the color fields in each chain neutralize via pair production over a distance scale proportional to the energy of the projectile parton that formed that chain (see Sec. IV). The spectator partons also drag a string behind them[23] that neutralizes over a large distance scale. That neutralization and recombination process is assumed to produce the leading secondaries, including the leading proton.

The crux of the problem is to specify how the parton filter works, i.e., what is the distribution of energy fractions of the partons that interact in the target. That distribution specifies the stopping power of high-energy protons, the information that we want to extract from the pA data. In order to characterize that distribution in terms of as few parameters as possible we adopt the simple algorithm proposed in Ref. 9. That algorithm specifies that the energy fraction of interacting partons falls off according to a geometrical progression,

$$\bar{x}_i=\alpha^{i-1}/(1+\alpha)^i,$$

where $\alpha\geq 1$ is the phenomenological parameter of the model. We adopt this algorithm mainly because of the simplicity of the resulting formalism in the next subsection and because it can adequately account for the A dependence of the current data. In Sec. VI we check that our conclusions about nuclear stopping power are relatively model independent by refitting the data in terms of a model with different assumptions.

B. Formalism

We translate now the above assumptions into the equations that define the model. First, we consider the invariant proton inclusive cross section. Assumption 1 on transverse factorization implies that

$$E\frac{d^3\sigma^{pA\to pX}}{dp^3}=\sigma_{\rm abs}(A)r_p g(p_\perp)\frac{dN}{dy}(A), \tag{2.2}$$

where $\sigma_{\rm abs}$ is the absorption cross section, r_p is the final proton-to-baryon ratio, $g(p_\perp)$ is the normalized transverse-momentum distribution, and dN/dy is the normalized rapidity density. We note that the present data[7] shows that $r_p g(p_\perp)$ is independent of atomic number and rapidity for $x>0.3$ and $p_\perp\sim 0.3$ GeV/c within 20% accuracy.

Assumption 2 allows us to decompose dN/dy into a standard multiple-collision series

$$\frac{dN}{dy}=\sum_{n=1}^{A} P_A(n)Q_n(x,x_0) , \tag{2.3}$$

where $P_A(n)$ is the Glauber probability[24] that n target nucleons interacted with the incident proton:

$$P_A(n)=\int \frac{d^2b}{\sigma_{\rm abs}(A)} \frac{A!}{(A-n)!n!}[N_A(b)/A]^n \times[1-N_A(b)/A]^{A-n} , \tag{2.4}$$

with $N_A(b)$ being the average number of interacting target nucleons at impact parameter b as given by

$$N_A(b)=\sigma_{\rm in}^{pN}\int dz\,\rho_A(z,b) . \tag{2.5}$$

Note that realistic nuclear densities, ρ_A, lead to rather large values of the single collision probability ($\gtrsim 0.2$) even for the heaviest nuclei due to their diffuse surfaces. In terms of $N_A(b)$ we can also express

$$\sigma_{\rm abs}(A)=\int d^2b\{1-[1-N_A(b)/A]^A\} . \tag{2.6}$$

Assumptions 3 and 4, concerning the separation of the reaction into two stages, imply that the probability density, $Q_n(x,x_0)$, of finding a proton with light-cone fraction x after n target nucleons have been struck can be written as

$$Q_n(x,x_0)=\int_x^1 dx' F_{n-1}(x',x_0) f_p(x/x',x_0/x') , \tag{2.7}$$

where $F_n(x,x_0)$ is interpreted as the probability density that the spectator projectile partons retain a light-cone fraction x after n projectile partons have interacted in the target. With the definition

$$F_0(x,x_0)=\delta(x-1) ,$$

the function $f_p(x,x_0)$ must correspond to the invariant distribution of protons in pN collisions at incident rapidity $y_0=\ln(1/x_0)$. A convenient parametrization of the $p+N\to p+X$ data is

$$f_p(x,x_0)=x/(1-x_0) . \tag{2.8}$$

We emphasize that our model says nothing about the fragmentation function $f_p(x)$. Our model only specifies the A dependence of pA reactions using pp reactions as input.

Since x_0 is the minimum light-cone fraction in the target frame, these functions are normalized as

$$\int_{x_0}^1 \frac{dx'}{x'} Q_n(x',x_0)=1 , \tag{2.9}$$

$$\int_{x_0}^1 \frac{dx'}{x'} f_p(x',x_0)=1 , \tag{2.10}$$

$$\int_{x_0}^1 dx' F_n(x',x_0)=1 . \tag{2.11}$$

Note that the scaling assumption 5 holds strictly only at asymptotic energies where $x_0\to 0$. For finite energies we include only the minimal dependence of these functions on x_0 required by overall energy conservation as in Ref. 21.

Note that Eq. (2.7) neglects the contribution from target fragmentation. To motivate this, recall that empirically the recoil proton in pp collisions is distributed as Consequently, for the rapidity range of interest, $y\gtrsim 4$, there is less than a five percent contribution to dN/dy from target recoil nucleons. Baryon pair production is also negligible for the energies considered here.

The dynamical information in this model is contained in the dependence of F_n on n. For simplicity we adopt the scaling algorithm of Ref. 9:

$$F_n(x,x_0)=\int_x^1 \frac{dx'}{x'} K(x/x',x_0/x') F_{n-1}(x',x_0) , \tag{2.12}$$

where $K(z,z_0)$ is a scattering kernel that specifies the probability density that a projectile proton carrying a light-cone fraction $1-z$ of the available light-cone energy $E^+=m_\perp/z_0$ interacts with a target parton.

Following Ref. 9 we parametrize K as

$$K(z,z_0)=\frac{\alpha z^{\alpha-1}}{1-{z_0}^\alpha} , \tag{2.13}$$

which is obviously normalized as

$$\int_{z_0}^1 dz\,K(z,z_0)=1 . \tag{2.14}$$

All the dynamical information in this model is therefore contained in the one parameter α. As we show in the next subsection in terms of α the fractional energy loss per interaction is $1/(1+\alpha)$, and the final baryon rapidity loss per interaction is $1/\alpha$. Since Eq. (2.12) leads to a geometrically decreasing fractional energy left in the spectator parton cloud as a function of the interaction number, we refer to it as a "geometrical" filter. It is important to emphasize that Eq. (2.12) says nothing about the space-time points of the n interactions. It is a purely momentum space equation. In Sec. IV we will consider possible extensions of this model to coordinate space. However, for the analysis of the pA data we do not yet need to specify the space-time picture behind (2.12).

With Eq. (2.13), the solution to Eq. (2.12) for $n\geq 1$ is

$$F_n(x,x_0)=\frac{1}{(n-1)!}\frac{\alpha x^{\alpha-1}}{1-{x_0}^\alpha}\left[\ln\left[\frac{1-{x_0}^\alpha}{x^\alpha-{x_0}^\alpha}\right]\right]^{n-1} . \tag{2.15}$$

We can now compare our model to others in the literature. In Ref. 21 only the case $\alpha=1$ was considered. That corresponds to the incoherent cascade limit where each interaction in the target is treated as if it were a pN collision in free space. In Ref. 22 the same ansatz for $K(z,0)$ was used, but in that model the two stages of the reaction in assumption 3 were not considered. Therefore, their formalism could not be directly applied to $pA\to cX$, where x is any other fragment than a proton. In Refs. 19 and 20 a different parametrization,

$$K(z,0)=1-\lambda+\lambda\delta(1-z) ,$$

was used but in a formalism that treats pp and pA on different footings and pion and proton production on different footings.

It is also instructive to compare the geometrical algorithm in Eq. (2.12) with one corresponding to a perhaps more intuitive "arithmetic" filter. The arithmetic filter is

one where the probability that n partons interact with energy fractions $x_1, \ldots, x_n$ can be expressed as an uncorrelated product

$$\propto W(x_1)\cdots W(x_n)\delta(1-x_1-\cdots-x_n) . \tag{2.16}$$

With Eq. (2.16), all n interacting partons carry the *same* average energy fraction, $\bar{x}_n$. Only energy conservation forces $\bar{x}_n$ to decrease with increasing n. This corresponds to the equipartition model 1 in Ref. 9. In terms of $W(x)$, $F_n(x)$ would then be given by

$$F_n(x)=\mathcal{N}_n \int dx_1\cdots dx_n W(x_1)\cdots W(x_n) \times\delta(1-x-x_1-\cdots-x_n) . \tag{2.17}$$

We refer to this as an arithmetic filter because the average energy fraction retained by the spectator partons after n interactions decreases approximately linearly with n rather than geometrically. However, because of the awkwardness of the delta function constraint above, analytic formulas for the arithmetic filter are rather cumbersome. The geometric filter has the advantage of incorporating energy conservation in a simple manner analytically. Otherwise, there is no deep reason to prefer the geometrical filter over the arithmetical one.

An important advantage of the present formalism is that by incorporating assumption 3 into Eq. (2.7) we treat $p+A\to c+X$ for any fragment c and any nucleus $A\geq 1$ on the same footing and that one parameter α fixes all those reactions. The basic inputs to this model are the measured $p+p\to c+X$ distributions and the known nuclear geometries. The multi-chain model is then a convenient extrapolation tool for pA and AB collisions with the absolute minimum of parameters. That at least one parameter is needed was shown by Wong[21] by the inability of the incoherent cascade model ($\alpha=1$) to fit the new data.[7] As we show in Sec. III one parameter, $\alpha\approx 3$, is in fact enough to fit the 100-GeV data.

Unlike the leading proton which is assumed to emerge only from the recombination of the projectile spectator partons, energetic pions can emerge not only from that fragmentation process but also from the hadronization of target chains. This is because pair production near the end of target chains can easily lead to meson formation and only much less frequently to baryon formation. In analogy to Eqs. (2.2), (2.3), and (2.7) we therefore have

$$E\frac{d^3\sigma^{pA\to\pi^\pm X}}{dp^3}=\sigma_{\rm abs}(A)g_\pi(p_\perp) \times\sum_{n=1}^{A}P_A(n)\left[Q_n^{\pi^\pm}(x)+\sum_{i=1}^{n-1}T_i^{\pi^\pm}(x)\right] , \tag{2.18}$$

where $Q_n^{\pi^\pm}$ includes the fragmentation of the projectile as well as the hadronization of the last chain, and T_i describes the hadronization of the ith target chain. Suppressing the x_0 dependences of all functions we can write

$$Q_n^{\pi^\pm}(x)=\int_x^1 dx' F_{n-1}(x')f_{\pi^\pm}(x/x') . \tag{2.19}$$

Since $F_0(x)=\delta(1-x)$, we see that f_π corresponds to the rapidity density of pions in $pp\to\pi X$. For simplicity we parametrize that data as

$$f_\pi(x)=c_1(1-x)^{a_1}+c_2(1-x)^{a_2} . \tag{2.20}$$

Again we emphasize that our model says nothing about the fragmentation functions $f_c(x)$. Those must be taken directly from $pp\to cX$ data. Only the $F_n(x)$ are specified in our model.

With the above parametrization, the first term with $a_1\approx 3$ represents the contributions from projectile fragmentation, and the second term with $a_2\approx 9$ represents the contribution from the hadronization of the target chain. With this interpretation, T_i in Eq. (2.18) is given by

$$T_i(x)=\int_x^1 dx' F_{i-1}(x')c_2(1-x/x')^{a_2} . \tag{2.21}$$

C. Measures of stopping power

We can now apply the above formalism to evaluate several measures of nuclear stopping power. One important measure is the mean rapidity loss $\langle\Delta y\rangle_z$ suffered by a baryon after having traversed a thickness z of nuclear matter at saturation density, $\rho_0=0.145$ fm^{-3}. Another important measure is the average fractional energy, $\langle x\rangle_z$, retained by the projectile spectator partons after traversing a thickness z.

We denote the average of a function of x over a normalized distribution $D(x)$ by

$$\langle g(x)\rangle_D=\int_{x_0}^1\frac{dx}{x}g(x)D(x) . \tag{2.22}$$

The average of that function as a function of atomic weight is then

$$\langle g(x)\rangle_A=\sum_{n=1}^{A}P_A(n)\langle g(x)\rangle_n , \tag{2.23}$$

where $\langle g(x)\rangle_n$ is given by Eq. (2.22) with $D(x)=Q_n(x)/x$. In order to evaluate averages as a function of nuclear thickness z, we use the Poisson limit of the binomial distribution to specify fluctuations of the collision number to get

$$\langle g(x)\rangle_z=e^{-z/\lambda}\left[g(1)+\sum_{n=1}^{\infty}\frac{(z/\lambda)^n}{n!}\langle g(x)\rangle_n\right] , \tag{2.24}$$

in terms of the proton mean free path λ.

We consider here only the high-energy limit $x_0\to 0$. In that limit we have

$$\langle x^m\rangle_{F_n}=\langle x^m\rangle_K\langle x^m\rangle_{F_{n-1}}=\left[\frac{\alpha}{\alpha+m}\right]^n , \tag{2.25}$$

$$\langle x^m\rangle_n=\left[\frac{\alpha}{\alpha+m}\right]^{n-1}\frac{1}{m+1} . \tag{2.26}$$

We see from Eq. (2.26) that the case $\alpha=1$ indeed corresponds to the incoherent cascade limit where in particular $\langle x\rangle_n=(\frac{1}{2})^n$. This relation also shows that the fractional energy loss of the projectile parton cloud per collision is just $1/(1+\alpha)$. Applying Eq. (2.25) for $n=m=1$, we see

that the spectator partons retain a fraction $\alpha/(1+\alpha)$ of the incident energy. The final baryon after recombination, however, is observed in pp collisions on the average with $\langle x\rangle_1 \approx \frac{1}{2}$. Therefore, the recombination process must leave the final baryon with a fraction

$$m_N/m^* \equiv (1+\alpha)/(2\alpha)$$

of the energy of the spectator partons. This shows how the effective mass m^* of the spectator parton cloud must depend on α in our model.

Equation (2.25) also shows that the average energy fraction $\bar{x}_i$ of the ith chain in this model falls off according to

$$\bar{x}_i = \langle x\rangle_{F_{i-1}} - \langle x\rangle_{F_i} = \alpha^{i-1}/(1+\alpha)^i \,. \tag{2.27}$$

Calculating next the average rapidity-loss moments, we find that in the $x_0 \to 0$ limit

$$\langle \Delta y\rangle_n = -\left\langle \ln\left[\frac{m}{m_\perp}x\right]\right\rangle_n$$

$$= (n-1)\langle \Delta y\rangle_K + \langle \Delta y\rangle_{f_p}$$

$$= (n-1)/\alpha + 1 \,, \tag{2.28}$$

$$\langle \Delta y^2\rangle_n = n(n-1)/\alpha^2 + 2(n-1)/\alpha + 2 \,, \tag{2.29}$$

where we neglected terms of order $\ln(m/m_\perp)$. The average rapidity-loss moments for impact-parameter-averaged pA collisions is then just given by the above expressions with n and n^2 replaced by their averages, $\langle n\rangle_A \equiv \nu_A$ and $\langle n^2\rangle_A$ over $P_A(n)$, respectively.

The average rapidity loss as a function of nuclear thickness is given by

$$\langle \Delta y\rangle_z = \frac{1}{\alpha}\frac{z}{\lambda} + \frac{\alpha-1}{\alpha}(1-e^{-z/\lambda}) \,, \tag{2.30}$$

$$\langle \Delta y^2\rangle_z = \frac{1}{\alpha^2}\left[\frac{z}{\lambda}\right]^2 + \frac{2}{\alpha}\frac{z}{\lambda} + \frac{\alpha-1}{\alpha}2(1-e^{-z/\lambda}) \,. \tag{2.31}$$

These relations show that $1/\alpha$ is the mean rapidity loss per interaction.

Finally, we note that the average fractional momentum carried by the spectator projectile partons after traversing a nuclear thickness z is given by

$$\langle x\rangle_z = \exp\left[-\frac{z}{(1+\alpha)\lambda}\right] \,. \tag{2.32}$$

The leading baryon ends up with only a fraction

$$m_N/m^* = (1+\alpha)/(2\alpha)$$

of that energy because of the effective mass of the spectator parton cloud.

III. EMPIRICAL STOPPING POWER OF NUCLEI

A. Nuclear geometry

The use of accurate nuclear densities to compute $P_A(n)$ in Eq. (2.4) is important because the $x \to 1$ limit of the proton inclusive cross section is directly proportional to $P_A(1)$:

$$\lim_{x\to 1} x\frac{dN}{dx} = P_A(1) \,. \tag{3.1}$$

Therefore, the nondiffractive component to the leading-proton rapidity density near the kinematic limit is fixed by geometry alone and is independent of the dynamics. Since sharp sphere approximations to nuclear densities grossly underestimate the probability that only one interaction occurs in heavy nuclei, simplified treatments of nuclear geometry could lead to erroneous dynamical information from $x \gtrsim 0.3$ data.

A sufficiently accurate approximation to nuclear densities is given by the Wood Saxon form

$$\rho_A(r) = \bar{\rho}_A\{1+\exp[(r-R_A)/d]\}^{-1} \,, \tag{3.2}$$

where $\bar{\rho}_A$ is determined by normalization, and the parameters R and d are chosen as

$$R_A = 1.19A^{1/3} - 1.61A^{-1/3} \text{ fm} \,, \tag{3.3}$$

$$d = 0.54 \text{ fm} \,. \tag{3.4}$$

We compared $P_A(n)$ computed with the above density to those computed by Sato[25] using density-dependent Hartree-Fock theory and found agreement within 10% accuracy. We chose $\sigma_{\text{in}}^{pN} = 32$ mb as the inelastic pN cross section. Furthermore, Table I shows that this density leads via Eq. (2.6) to satisfactory agreement between the calculated and measured[26] reaction cross sections. Also listed in the table are values of $P_A(1)$, $P_A(2)$, and $\nu_A \equiv \langle n\rangle_A$ for various nuclei. In practice, we terminated the series in Eq. (2.3) at $n=15$.

For comparison, we note that the densities employed in Ref. 21 lead to 10% larger values of $P_A(1)$ and $\sigma_{\text{abs}}(pA)$. This led to invariant cross sections that are 20% larger than ours at high x. In the calculations of Ref. 19 only the term $n = \langle n\rangle_A$ was considered in Eq. (2.3). The neglect of surface and fluctuation effects is partially responsible for the large (17-fm) momentum-degradation length that was obtained in Ref. 19. In Ref. 20 diffuse surface effects were neglected, but since their method treated pp and pA collisions differently, they were able to fit the data by introducing a normalization factor. Finally, we note that in the pioneering work of Ref. 17 only a very crude treatment of geometry was considered. An important object of the present work is to reduce the uncertainties associated with such trivial geometrical effects.

B. Implications of 100-GeV proton spectra

In Fig. 1 we compare our calculated invariant proton inclusive cross sections to the data[7] at 100 GeV. For these calculations we used the parametrization of the transverse-momentum distribution of Ref. 9 and took the proton-to-baryon ratio $r_p = 0.53$. This gives $r_p g(p_\perp) = 0.8876$ for the $p_\perp = 0.3$ GeV/c relevant to the data.

In Fig. 1 the case $\alpha = 1$ verifies the finding of Wong[21] that the incoherent cascading cannot account for the A dependence of the data. The data indicate that the proba-

TABLE I. Reaction cross sections and Glauber probabilities.

A	σ_A (expt) (mb)	σ_A (theo) (mb)	$P_A(1)$	$P_A(2)$	ν_A
12	222	225	0.57	0.25	1.7
27	409	411	0.45	0.24	2.1
64	764	765	0.34	0.22	2.7
108	1101	1105	0.28	0.19	3.1
207	1730	1726	0.22	0.15	3.8

bility of small energy loss is greater than predicted by incoherent cascade. The partial transparency of nuclei can be parametrized in our model by setting $\alpha > 1$. Taking into account the uncertainties associated with our model assumptions and those of the data, we see that

$$\alpha = 3 \pm 1 \tag{3.5}$$

leads to a satisfactory fit to the A dependence of the data over the measured x region. Note that the $x=1$ intercept is independent of α in accord with Eq. (3.1). This value of α is in agreement with the value deduced in Refs. 20 and 22 using a less general formalism.

To emphasize the limited kinematic domain covered by the present data, we show in Fig. 2 the normalized rapidity distributions for $\alpha=3$. We also calculated dN/dy for collisions with the outer (dashed) and inner (dashed-dot) halves of the nucleus for comparison to the extrapolations by Busza and Goldhaber.[17] This separation into inner and outer half is accomplished by restricting the range of impact-parameter integration below and above the impact parameter b_c corresponding to one half of the reaction cross section. Comparing the dashed-dot curve in Fig. 2(b) with the corresponding one in Fig. 3 of Ref. 17 we find a substantial difference. The peak of our curve is shifted by one unit of rapidity less than their extrapolation. This is a consequence of their cruder treatment of geometry and their constraint that dN/dy vanish at $x=1$. It would be very useful to measure the multiplicity dependence of the proton distributions to test more severely these geometrical effects.

Having determined the range of α compatible with the proton yields, we show the average rapidity loss, $\langle \Delta y \rangle_z$, as a function of nuclear depth in Fig. 3. While we differ with the extrapolated distributions of Ref. 17 for the inner-half impact parameters, we find in agreement with Ref. 17 that the maximum rapidity shift induced by heavy nuclei is

$$\Delta y_{\max} \approx \langle \Delta y \rangle_{z\sim 14\ \mathrm{fm}} \approx 2.5 \pm 0.5 \ . \tag{3.6}$$

This rapidity shift may occur when a proton traverses the entire diameter of a heavy nucleus. It is important to keep in mind, however, that the above extrapolation has

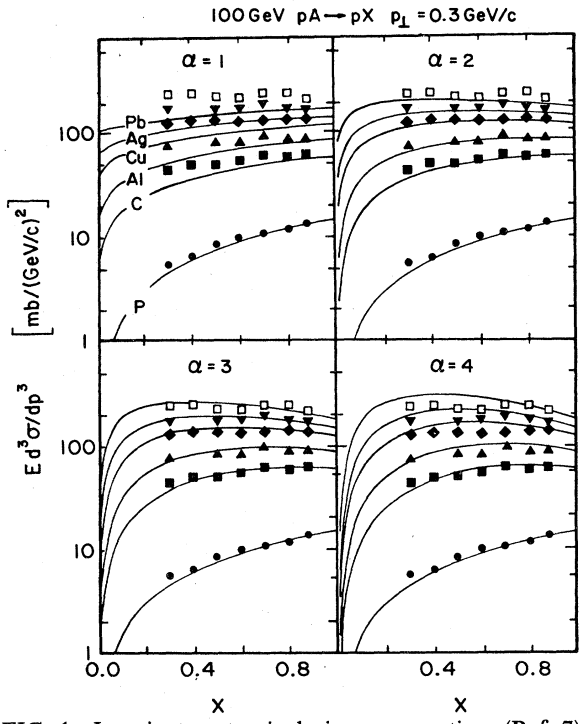

FIG. 1. Invariant proton inclusive cross sections (Ref. 7) for $p+A \to p+X$ at 100 GeV as a function of light-cone x for fixed $p_\perp = 0.3$ GeV/c. Solid curves are calculated using the multichain model. The incoherent cascade (Ref. 21) corresponds to the curves for $\alpha=1$. The effect of increasing nuclear transparency is shown by cases $\alpha=2$, 3, and 4. Note that pp and pA are treated on the same footing.

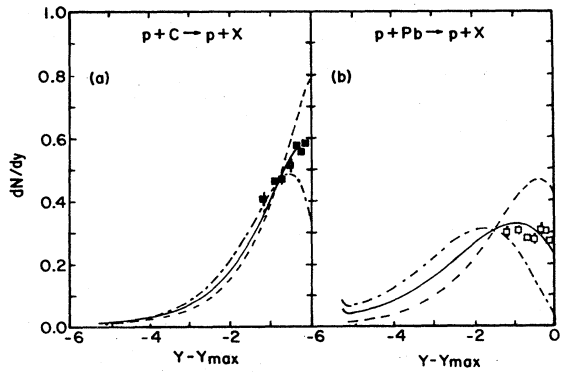

FIG. 2. Leading-proton rapidity density as a function of rapidity measured in projectile frame. All curves correspond to $\alpha=3$ and the C and Pb target data are deduced from Ref. 7 assuming $r_p g(0.3) = 0.8876$. Solid curves are for impact-parameter-averaged results, while dashed and dashed-dot curves correspond to outer-half ($b > b_c$) and inner-half ($b < b_c$) collisions, respectively. Here b_c is chosen to be the impact-parameter cut leading to $\frac{1}{2}$ of the reaction cross section as in Ref. 17.

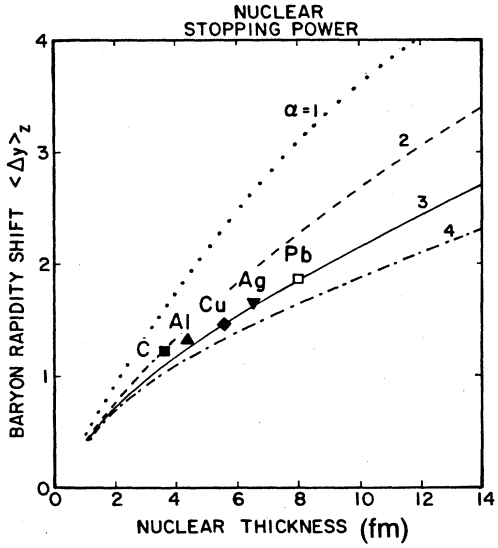

FIG. 3. Stopping power of nuclear matter as measured by the mean baryon rapidity shift as a function of nuclear thickness. This is the asymptotic rapidity shift (see Sec. IV). Curves for $\alpha=1-4$ are shown. Symbols indicate the impact-parameter-averaged mean rapidity shifts for the case $\alpha=3$ for finite nuclei as a function of the average nuclear thickness, $\nu_A\lambda$.

yet to be tested experimentally by more detailed measurements involving associated multiplicity triggers. The impact-parameter-averaged data yield $\langle \Delta y \rangle_A$ as indicated by the symbols in Fig. 3. For finite nuclei we took the average nuclear depth to be $z=\nu_A\times 2.08$ fm. The Pb data thus only tests nuclear stopping to average depths of ~ 8 fm.

C. Consistency with pion spectra

To check the consistency of our model we compare next the calculated invariant pion inclusive cross sections with data. For these calculations we used the following fit to the $pp\to\pi^{\pm}X$ data:

$$\sigma_{\rm in}^{pN} g_\pi(0.3) f_{\pi^-}(x)=[35(1-x)^9 + 18(1-x)^{2.8}]\ \text{mb/GeV}^2\ , \quad (3.7)$$

$$\sigma_{\rm in}^{pN} g_\pi(0.3) f_{\pi^-}(z)=[31.8(1-x)^{8.6} + 4.59(1-x)^{3.29}]\ \text{mb/GeV}^2\ . \quad (3.8)$$

The $pp\to\pi$ data were fit with this functional form to allow for a simple calculation of the target-chain contributions $T_i(x)$ in Eqs. (2.18) and (2.21).

In Fig. 4 we see that the A dependence of the π^- is well accounted for in the measured x region. However, we see that while the A dependence of the π^+ spectra is reproduced for $A>12$, the $pp\to\pi^+X$ data are systematically lower than the solid curve which is obtained in this case by demanding the best overall fit to the nuclear data. Conversely, if we insisted on fitting the pp data by reducing the normalization in Eq. (3.7) by a factor $\sim\frac{2}{3}$, then all the calculated nuclear curves would be systematically below the data. Private communication with W. Busza

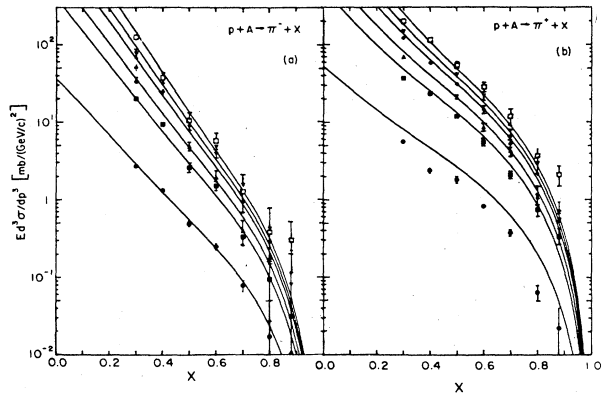

FIG. 4. Inclusive $p+A\to\pi^{\pm}+X$ cross sections (Ref. 7) at 100 GeV for $p_\perp=0.3$ GeV/c. All calculated curves correspond to $\alpha=3$.

indicated that it is possible that for the reaction $p+p\to\pi^++X$ certain experimental systematic effects could lead to underestimating the normalization in this channel. Another reason why $pA\to\pi^+$ data may require a larger $pN\to\pi^+$ is the apparent isospin dependence of π^+ production. It was noted in Ref. 21 that in the region $x>0.3$ the $pn\to\pi^+$ cross section is about a factor of two greater than the $pp\to\pi^+$ cross sections. While those data are also suspect, such an isospin effect could account for the difference between the $pp\to\pi^+$ data and the solid curve. On the other hand, it appears[21] that the $pp\to\pi^-$ and $pn\to\pi^-$ cross sections are approximately the same. Thus, no isospin effect is expected in that channel.

Finally, we note that the $pA\to\pi^+$ data at $x\approx 0.9$ are systematically higher than the calculations. This is likely to be due to the neglect of diffractive contributions in our model.[13] Such diffractive contributions would be expected also in $p+A\to n+X$.

The successful reproduction of both the normalization and the shapes of the pion yields should be contrasted with the incoherent cascade model[21] that overpredicted those yields by a factor of 7. This is due to the neglect of longitudinal growth in the cascade model. Our starting point via Eq.(2.18) implicitly incorporates that effect by including only one projectile fragmentation process according to assumption 3 in Sec. II A. Unfortunately, this high-x kinematical domain is not very sensitive to the multichain aspect of our model. Target chains produce pions mostly in the $x<0.3$ region. On the plus side, the data are, however, sensitive to the energy-loss mechanism since the ratio of pion cross sections for Pb and p targets varies by a factor of three in the measured x region for π^-. The agreement of our calculations with the pion data shows that the energy loss of a proton deduced by fitting the proton data with $\alpha=3$ is consistent with both the leading pion and proton spectra.

D. Deviations from scaling

While we have seen that the 100-GeV/c data on leading protons and pions could be well reproduced in our model by one fixed parameter, $\alpha\approx 3$, the scaling assumption

must break down at sufficiently low energy. In Fig. 5 we compare our calculations for $p+A \to p+X$ with data[27] taken at 24 GeV. For that calculation we took $r_p=0.75$ and $g(p_\perp)$ from a fit to the 24-GeV $pp \to pX$ data of Blobel *et al.*[28] The data and calculations correspond to fixed angle $\theta=17$ mr. The three curves show cases $\alpha=1$ (solid), 3 (dashed), and 6 (dot-dashed). While none of the curves provides a good fit, the data seem to indicate a bigger energy loss than expected from the $\alpha=3$ curve (i.e., the integral of the measured distributions between $0.1<x<1$ is less than the integral of the calculated distributions). Further support for this conclusion has come from preliminary $pA \to pX$ data[29] at 17 GeV, where the normalization of the high-x proton density seems to be in fact a factor of two smaller than that of the data displayed in Fig. 5.

These data therefore indicate that the stopping power of nuclei at ~ 20 GeV is greater than at 100 GeV. In terms of our phenomenological parameter α, a value closer to unity may be necessary at these lower energies. For the purposes of the present paper, we shall not try to incorporate such scaling violations by modifying the model but only note their existence. Fortunately, we find in the next section that our conclusions about stopping domain of nuclear collisions are not especially sensitive to such violations.

IV. SPACE-TIME DEVELOPMENT OF STOPPING

A. Momentum-degradation length

From the pA data we could deduce how much energy is lost by the leading baryon *after* traversing a certain thickness of nuclear matter. Our analysis confirms earlier estimates[7,19–22] that about 90% of the incident energy of a proton could be lost after traversing 14 fm of nuclear matter. However, until now the question of *where* that energy is deposited has not been seriously addressed. Obviously, the data provide constraints only on the momentum space aspects of models, which in our case is the value of α. The space-time development of stopping and energy deposition is largely unconstrained by the available data. However, for applications to nuclear collisions it is necessary to know not only how much energy is lost but also where that energy is deposited. In this section we consider the space-time picture of energy loss and deposition in the context of the multichain model. We pay particular attention to the effect of time dilation and longitudinal growth[2–4] on the space-time development of particle production. We show below that this basic phenomenon, neglected in previous studies on stopping power, limits the maximum energy that can be deposited into a nucleus. Furthermore, that maximum energy deposition is relatively insensitive to dynamical assumptions.

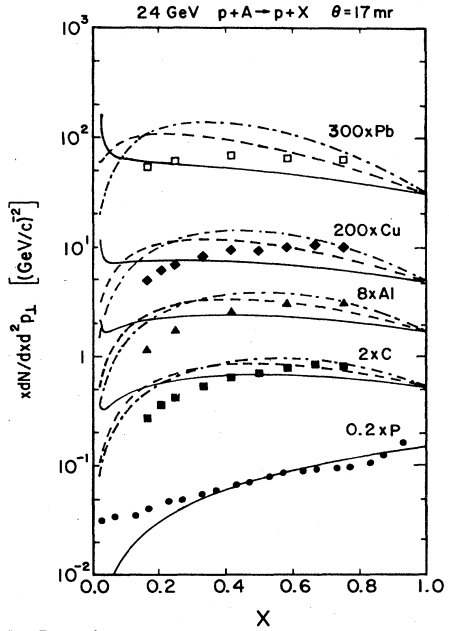

FIG. 5. Invariant proton inclusive distributions (Ref. 27) at 24 GeV for fixed angle, $\theta=17$ mr. Calculations for $\alpha=1$, 3, and 6 are shown by solid, dashed, and dashed-dot curves, respectively. The pp data are from Ref. 28.

Taking fluctuations of the number of interactions into account, we found in Eq. (2.32) that the average energy fraction retained by the spectator projectile partons decreases exponentially with nuclear thickness traversed. This implies that

$$\frac{dE}{dz} \approx -\frac{E}{\Lambda_p} , \tag{4.1}$$

where $E(z)$ is the energy left in the projectile spectator cloud at depth z in the matter, and Λ_p is the "momentum-degradation length"[20] as given by

$$\Lambda_p=(1+\alpha)\lambda \approx 8\pm 2 \text{ fm} . \tag{4.2}$$

If we ignore fluctuations as in Ref. 20, then $1+\alpha$ above is replaced by $1/\ln(1+1/\alpha)$. For $\alpha=3$ fluctuations enhance Λ_p by only 15%.

While Eq. (2.32) relies on the assumption that the stopping dynamics scales with energy, Eq. (4.1) is more general if we let Λ_p depend on energy. The value of Λ_p in Eq. (4.2) has been deduced from data at laboratory energies ~ 100 GeV. For lower energies we expect according to Fig. 5 that Λ_p decreases as α decreases. For comparison, our value of Λ_p is a factor of two larger than if incoherent cascading were valid.[21] It is also 60% larger than deduced in Ref. 20 because they neglected fluctuations and used the total rather than the inelastic pp cross section for estimating λ (their revised results, to be published, are in accord with ours). On the other hand, our value is a factor of two smaller than deduced by Hwa,[19] where only the roughest geometrical considerations and dynamical approximations[20] were considered.

Stopping the baryon in a frame that moves with rapidity y with respect to the laboratory means that E in the laboratory is reduced to $m^* \cosh(y)$, where m^* is an effective mass. Recall from Sec. II C that in our model the fraction of the energy of the spectator partons that is carried away ultimately by a baryon is

$$f=(1+\alpha)/(2\alpha) \approx \tfrac{2}{3} .$$

By defining $m^*=m_N/f$, we thus guarantee that on the average the projectile nucleon ends up at rest in that frame. Since $E(z)=E_0e^{-z/\Lambda_p}$ from Eq. (4.1), the thickness of nuclear matter required to reduce the rapidity of a nucleon from y_0 to y is

$$L(y)\approx\Lambda_p(y_0-y-\delta y)\ , \tag{4.3}$$

where $\delta y=\ln(1/f)\approx 0.4$. For $y=0$ the approximation $E\approx m_\perp e^y/2$ used in Eq. (4.3) is not good enough. The stopping distance in the laboratory frame is given rather by

$$L(0)\approx\Lambda_p\ln(E_0/m^*)\ . \tag{4.4}$$

Solving for $\Delta y=y_0-y$ from Eq. (4.3), we note that $\Delta y=L/\Lambda_p+\delta y$ increases slower with L than if we used $\langle\Delta y\rangle_L$ from Eq. (2.30). This is because the distribution of energy loss is so wide that the average rapidity loss tends to overestimate the average energy loss for a given α. Within the large uncertainties in the present determination of α, however, this distinction is not so crucial. To be on the conservative side we use Eq. (4.3) in applications to nuclear collisions.

For application to collisions of symmetric nuclei $(A+A)$, we are interested in reducing the incident rapidity by only $\frac{1}{2}$ since such a rapidity shift applied to both target and projectile nucleons would lead to stopping of all baryons in the center-of-mass system. The thickness of nuclear matter required to stop baryons in the c.m. system is thus estimated to be

$$L^*=L(y_0/2)=\Lambda_p(y_0/2-\delta y)\ . \tag{4.5}$$

B. Effect of longitudinal growth

We now turn to the problem of how to reconcile the slow $(\ln E_0)$ increase of these stopping distances with the concept of longitudinal growth.[2] Because of Lorentz time dilation, the formation time of a secondary particle increases linearly with the energy of that particle.[3] Therefore, at a distance z into the matter only particles with rapidities[3,4]

$$y\lesssim\ln(2z/\tau_0)\ , \tag{4.6}$$

could have come on shell. The proper time for formation of hadrons is estimated to be $\tau_0\approx 1$ fm. Recall[2] that Eq. (4.6) also follows from the uncertainty principle in terms of light-cone variables $(x_\pm=t\pm z,\ q_\pm=E\pm q_z)$

$$\Delta x_\pm\gtrsim\frac{2\hbar}{\Delta q_\mp}\ . \tag{4.7}$$

Therefore the production of a particle with rapidity y and transverse mass $m_\perp$ cannot be localized on the average within a distance $\Delta z\sim e^y/m_\perp$ of the interaction point. Note that this is in spite of the fact that at any *fixed* time the z coordinate of a high-energy particle with a rapidity wave packet of width Δy can be measured with great accuracy, i.e.,

$$\Delta z\gtrsim 2\hbar/(m_\perp e^y\Delta y)$$

as $y\to\infty$. What we cannot localize well is the production point of the particle, not its wave packet once it has been formed. This exponential growth with rapidity of the uncertainty in the production point is referred to as longitudinal growth. We see that $\tau_0\approx 2/m_\perp\sim 1$ fm even for pointlike partons due to limited $p_\perp$ distributions. For pointlike particles the transverse Compton wavelength sets the minimum uncertainty in the proper time for its formation. Time dilation then increases the uncertainty in the formation time in any other frame.

To see what limitations longitudinal growth places on the energy deposited per unit length, let $P_f(z;y)\delta z$ be the formation probability of a secondary with rapidity y at some point between z and $z+\delta z$ downstream from the interaction point. A simple form of P_f that incorporates Eq. (4.6) is

$$P_f(z;y)=\frac{1}{2\chi l(y)}\theta(z-(1-\chi)l(y))\theta((1+\chi)l(y)-z)\ \underset{\chi\to 0}{\to}\ \delta(z-l(y))\ , \tag{4.8}$$

where $l(y)=\tau_0\sinh(y)\approx e^y/m_\perp$ is the average production point of a particle with rapidity y, and $\chi l(y)/\sqrt{3}$ is rms width of the production region. The parameter $\chi\lesssim 1$ controls the magnitude of fluctuations about the average production point.

For an interaction at point z_0, the energy deposited at z in the form of on-shell secondaries is

$$\frac{dE^\infty}{dz}=\int dy\,P_f(z-z_0;y)m_\perp\cosh(y)\frac{dN}{dy}\ , \tag{4.9}$$

where dN/dy is the final rapidity density of secondaries. Since the empirical dN/dy is only a slowly varying function of y in the central region, we see that longitudinal growth implies that dE^∞/dz is approximately a constant[30] given by

$$\sigma=\frac{m_\perp}{\tau_0}\left\langle\frac{dN}{dy}\right\rangle\frac{1}{2\chi}\ln\left[\frac{1+\chi}{1-\chi}\right]\sim 1\ \text{GeV/fm}\ . \tag{4.10}$$

Note that fluctuations around the average production point enhance dE^∞/dz.

The approximate constancy of dE^∞/dz also follows naturally from the string model. A string produced in a collision corresponds to a color flux tube that stretches out with time. The constant color-electric field $\mathscr{E}$ in that tube leads to a constant energy per unit length $\sigma\propto\mathscr{E}^2$. In the color fields of that tube the Schwinger mechanism produces pairs that neutralize the field. Since a particle with energy ϵ cannot be emitted from the string before the kinetic-energy loss σz exceeds ϵ, longitudinal growth is automatically satisfied. Furthermore, the empirical string tension, $\sigma\approx 1$ GeV/fm, gives an energy loss similar to Eq. (4.10).

The energy deposition per unit length can be approximately constant, of course, only over a finite range. That range is fixed simply by energy conservation. For a target chain carrying an energy fraction x, energy conservation fixes its "length," $l(x)$, to be

$$l(x)=xE_0/\sigma\ , \tag{4.11}$$

where E_0 is the incident energy. At the point where the string is stretched to length $l(x)$ all the kinetic energy of the leading parton has been converted into potential energy. That potential energy is in turn converted via the Schwinger mechanism into energy of pairs that are formed in the color neutralization process. A target chain formed at depth z_0 therefore leads to an approximately constant energy deposition per unit length over a finite range $z_0 < z < z_0 + l(x)$, so that

$$\frac{dE^{\infty}}{dz} \approx \sigma\theta(z - z_0)\theta(z_0 + l(x) - z) . \tag{4.12}$$

Summing over all target chains leads then to the estimate

$$\frac{dE^{\infty}}{dz} \approx \sigma\left\langle \sum_i \theta(z - z_i)\theta(z_i + l(x_i) - z)\right\rangle , \tag{4.13}$$

where the average denoted by angular brackets is over the multiplicity of target chains, their production points z_i, and their energy fractions x_i.

To Eq. (4.13) we must still add the contribution to the energy deposition due to the recombination and neutralization of the projectile chain. We do this formally by extending the sum from $i=0$ to $i=N$, where $i=0$ refers to the contribution of the projectile chain. Thus, z_0 is the point from which fragments from the projectile chain start to materialize, and $l(x_0) \equiv (1 - x_1 - \cdots - x_N)$ is the distance over which the projectile string neutralizes. With this convention, note that the total length of all chains is just the naive longitudinal length scale

$$\sum_{i=0}^{N} l(x_i) = E_0/\sigma . \tag{4.14}$$

From this it is clear that an important feature of multistring models is the occurrence of multiple length scales that are smaller than the naive length scale, E_0/σ.

What we must next specify is the distribution of $z_0, \ldots, z_N$ and $x_1, \ldots, x_N$ as well as of N. The distribution over N is given by a Poisson from Glauber theory, such that $\langle N \rangle = 2R/\lambda$, where $2R$ is the thickness of nuclear matter. The distribution of the fractional energies, $x_1, \ldots, x_N$, carried by the N target chains is completely specified in our model as

$$D_N(x_1, \ldots, x_N) = \frac{K(1-x_1)}{1} \frac{K((1-x_2)/(1-x_1))}{(1-x_1)} \cdots . \tag{4.15}$$

This distribution leads to the average fractional energies $\bar{x}_i$ of target chains given by Eq. (2.27).

The distribution of interaction points, z_i, on the other hand, is not specified by the model as formulated thus far. Fitting the momentum space data does not require knowledge about the z_i. Again we emphasize that those data provide information only on energy loss and not on energy deposition. Thus, strictly speaking the pA data are not enough to determine the energy deposition that is crucial to applications to nuclear collisions. Note that the maximum energy deposition in a finite nucleus is not even bounded by the energy loss because some of the energy carried by the spectator partons can also end up within the nucleus [term $i=0$ in (4.13)]. On the other hand, the energy deposition could be significantly smaller than the energy loss because the lengths of several chains could exceed the nuclear thickness. To estimate the energy deposition we consider two extreme models for the distribution of production points, z_i.

The first model for that distribution follows naturally from multiple collision theory. In such a framework interactions occur sequentially involving successively smaller and smaller energies. Therefore, the first chain, carrying on the average the highest energy fraction $\bar{x}_1 = 1/(1+\alpha)$, would be produced first ($z_1 \sim \lambda$). Then the second chain would be created after another mean free path, etc. Such a time-ordered sequence of interaction points corresponds to a distribution

$$S_N(z_1, \ldots, z_N; 2R) = \frac{N!}{(2R)^N} \theta(z_2 - z_1) \cdots \theta(z_N - z_{N-1}) , \tag{4.16}$$

where $2R$ is again the thickness of the nuclear slab and $0 < z_i < 2R$ for all i. With Eq. (4.16) the average production point of chain i is $\langle z_i \rangle = 2Ri/(N+1)$.

A second possibility for the distribution of interaction points is suggested by the parton model. In that model partons are assumed to have very large mean free paths. Only because there are so many of them can a few nevertheless interact inside a finite nucleus. In that picture the z_i are thus uniformly distributed over the nuclear thickness. Such a distribution thus corresponds to

$$S_N(z_1, \ldots, z_N; 2R) = (2R)^{-N} . \tag{4.17}$$

On the average, there is an interaction every $2R/(N+1)$ as with the time-ordered distribution (4.16). However, with (4.17) there is no correlation between the interaction point and the energy of the chain.

Clearly, (4.16) leads to an upper bound on the estimate for energy deposition, because the first few chains that carry the largest fractional energies have the longest range within the nuclear matter to neutralize. Conversely, (4.17) leads to a lower bound since some of the time the shorter chains are allowed to be produced before the longer ones. Comparing the energy deposition resulting from (4.16) with that resulting from (4.17) will give an indication of the theoretical uncertainty in those estimates.

Consider first the time-ordered case corresponding to (4.16). On the average, the energy of a chain produced at depth z is given by $E(z)/(1+\alpha)$. Therefore, its length is approximately

$$\bar{l}(z) = l_\alpha e^{-z/\Lambda_p} , \tag{4.18}$$

where $l_\alpha = E_0/[(1+\alpha)\sigma]$. Figure 6 illustrates the range of nuclear depths over which different target chains neutralize in this case. A given target chain n neutralizes on the average between $n\lambda \lesssim z \lesssim n\lambda + \bar{l}(n\lambda)$. Note that the length of all chains increases linearly with the incident energy and that those lengths are twice as long for the case $\alpha=1$ as for $\alpha=3$ because the average energy lost forming target chains is twice as large in the former case. The peculiar shape of the solid curves results from the interplay between the linear growing and exponentially de-

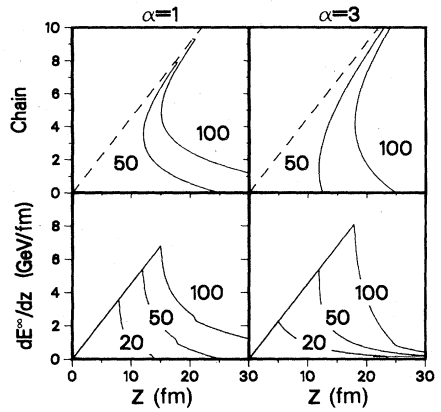

FIG. 6. Top graphs show the color-neutralization region of different target chains in the laboratory frame. Chain n is formed at depth $z=n\lambda$ (dashed line) and is neutralized between $n\lambda \le z \le z_c(n\lambda)$, where $z_c(z)$ (solid curves) is given by Eq. (4.13). The curves are labeled by the incident laboratory energy in GeV. The bottom two graphs show the energy *deposition* per unit length, Eq. (4.20) in the form of on-shell secondaries as a function of nuclear depth. The linear increase of dE^∞/dz up to some depth z^* given by Eq. (4.19) is a consequence of longitudinal growth and the approximate constancy of the rapidity density dN/dy of secondaries produced in the neutralization process. Comparing cases $\alpha=1$ (left side) and $\alpha=3$ (right side) shows that dE^∞/dz is not very sensitive to uncertainties in α.

creasing contributions to the end point of the neutralization range for different chains. For a fixed energy and α there exists a minimum depth z^* below which none of the chains have yet neutralized. That depth, as given by

$$z^*=\Lambda_p\left\{1+\ln\left[\frac{E_0}{(1+\alpha)\sigma\Lambda_p}\right]\right\}, \tag{4.19}$$

grows only logarithmically with incident energy.

Since each chain contributes approximately a constant σ to dE^∞/dz, we can estimate the total energy deposition per unit length by noting that a new chain is created on the average every mean free path λ and summing over all contributing chains via

$$\frac{dE^\infty}{dz}\approx\sigma\int_0^z\frac{dz_0}{\lambda}\theta[z_0+\bar{l}(z_0)-z]\ . \tag{4.20}$$

For $z<z^*$ the total energy deposited per unit length simply increases linearly,[30]

$$dE^\infty/dz\approx\frac{\sigma z}{\lambda},\quad z<z^*\ . \tag{4.21}$$

This linear growth is illustrated in the bottom part of Fig. 6. For $z>z^*$, dE^∞/dz decreases rapidly as fewer chains contribute. Note the little kink in the curves that occurs at

$$z=L(0)=\Lambda_p\ln(E_0/m^*)$$

corresponding to the stopping distance in the laboratory frame as given by Eq. (4.4). For $z>L(0)$ the integration over z_0 in Eq. (4.20) terminates at $L(0)$. Nevertheless, dE^∞/dz continues to be finite because not all target chains can neutralize so fast. For $E_0=50$ GeV and $\alpha=1$, for example, the baryon stops on the average at a depth $L(0)=17.5$ fm while target chains continue to produce secondaries until the first chain is neutralized at depth ≈ 25 fm. In this example linear growth of dE^∞/dz ceases at $z^*=12$ fm.

The most striking feature to note in Fig. 6 is the *insensitivity* of dE^∞/dz to the value of α. Even though the hadronization range of any particular chain is sensitive to α, the net sum of all chains is rather stable with respect to changing α. It is also obvious from the dE^∞/dz curves that the energy deposited per unit length eventually saturates as the incident energy increases. At a fixed depth z, dE^∞/dz saturates at $\sigma z/\lambda$ for incident energies satisfying $z^*>z$. Therefore, the total energy deposited within a finite nucleus of thickness $2R$ saturates at

$$E^\infty(2R)\le 2\sigma R^2/\lambda\ , \tag{4.22}$$

with the upper bound being reached at incident energy

$$E_0=E^{\rm sat}=\begin{cases}(1+\alpha)\sigma 2R & \text{if } 2R<\Lambda_p\ ,\\ (1+\alpha)\sigma\Lambda_p e^{(2R-\Lambda_p)/\Lambda_p} & \text{if } 2R\ge\Lambda_p\ .\end{cases} \tag{4.23}$$

The maximum energy that a proton can deposit in nuclear matter of thickness $2R=14$ fm is thus $E^\infty\approx 45$ GeV which is reached for incident energies $E_0>E^{\rm sat}\approx 60$–$80$ GeV for $\alpha\approx 1$–3.

Consider now the alternate possibility, Eq. (4.17), where the assumption about the time ordering of the production point z_i is removed. In this case, each z_i is uniformly distributed between $0<z_i<2R$. Consequently, chain i contributes to the energy deposition per unit length an amount

$$\left[\frac{dE^\infty}{dz}\right]_i\approx\sigma\int_0^{2R}\frac{dz_i}{2R}\theta(z-z_i)\theta(z_i+l(x_i)-z)\ . \tag{4.24}$$

This integral leads to a trapezoid shape in the range $0<z<2R+l(x_i)$. Of more interest, however, is the total energy deposition into nuclear matter of thickness $2R$. That is given by

$$E_i^\infty(2R)=\begin{cases}\sigma R, & l(x_i)>2R\\ \sigma l(x_i)[1-l(x_i)/(4R)], & l(x_i)<2R\ .\end{cases} \tag{4.25}$$

We see from (4.25) that at sufficiently high energies, when the $l(x_i)$ generally exceed $2R$ for every chain, the sum over the $\approx 2R/\lambda$ chains gives the same total energy deposition as in Eq. (4.22). Therefore, we draw the important conclusion that the maximum energy deposition in a finite nucleus neither depends on the distribution of the x_i *nor* on the distribution of the z_i. For a nuclear thickness of 14 fm, that maximum energy deposition is ~ 45 GeV. We note, however, that this estimate depends on the effective string tension $\sigma\approx 1$ GeV/fm and the assumption that the strings add incoherently. The assumption that strings add incoherently is justified only if the color electric charge at the end of the strings is random. Clearly, a random walk in color space leads to an average color electric field squared, $\langle \mathscr{E}^2\rangle$, that grows only linear-

ly with the number of interactions. Hence, the effective number of strings grows only linearly with nuclear depth although large fluctuations about the average can be expected.

While the maximum energy deposition asymptotically does not depend on the details of those distributions, the maximum energy deposition in the baryon stopping region does. That is because in the baryon stopping region, some of the chains have lengths less than $2R$, and therefore the energy deposition from those chains depends on their production points, z_i. The maximum energy deposition in the baryon stopping region is estimated in the next section.

C. The stopping domain of nuclear collisions

In the context of nuclear collisions we are interested in stopping baryons in the midrapidity or nucleon-nucleon center-of-mass system. The condition for stopping a nucleon in the midrapidity frame due to a zero impact-parameter collision with a nucleus of radius R is $L^* < 2R$, where L^* is given by Eq. (4.5). This limits the energy per nucleon in the center of mass to be

$$\gamma_{\text{c.m.}} m_N \lesssim m_N \cosh(2R/\Lambda_p + \delta y) \ . \tag{4.26}$$

Of course, the same condition is obtained by requiring that the stopping distance in the center-of-mass system be smaller than the Lorentz-contracted radius, $R/\gamma_{\text{c.m.}}$. For a finite impact parameter b, $2R$ is replaced by $2(R^2-b^2)^{1/2}$.

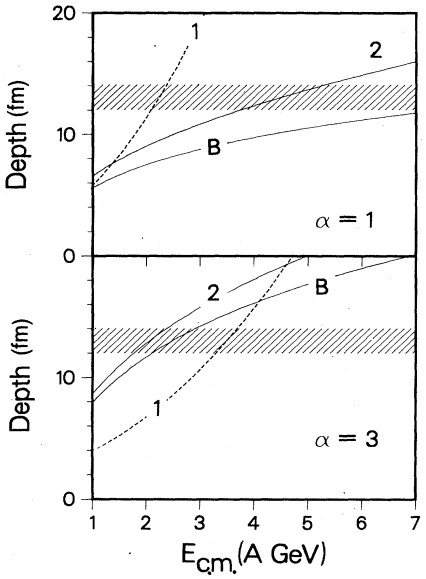

FIG. 7. The laboratory distance scales involved in stopping baryons and producing secondaries are shown as a function of center-of-mass kinetic energy for $\alpha=1$ and 3. Curve B gives the depth of nuclear matter, Eq. (4.5), required to halve the rapidity of the incident baryon. Curve 1 shows the extent of the hadronization region of the first target chain via Eq. (4.27). The hadronization of the last target chain occurs between curve B and curve 2 as given by Eq. (4.28). The crossing of the shaded region by any curve locates the end of the stopping domain of nuclear collisions. Below that point not only do most of the baryons stop but also most of the energetic secondary particles are produced within the Lorentz-contracted nuclear volume in the center-of-mass frame.

In Fig. 7 the thickness L^* of nuclear matter required to reduce the incident laboratory rapidity $2y_{\text{c.m.}}$ to $y_{\text{c.m.}}$ is shown by the solid curves labeled B for both $\alpha=1$ and 3. For $\alpha=3$, the c.m. stopping distance exceeds the diameter of the heaviest nuclei for $\gamma_{\text{c.m.}} \gtrsim 4$. For $\alpha=2$, $L^* > 14$ fm for $\gamma_{\text{c.m.}} > 6$. If we could extrapolate the $\alpha=1$ curve indefinitely, then $L^* > 14$ fm only for $\gamma_{\text{c.m.}} > 14$. Recall that $\gamma_{\text{c.m.}} \approx 6$ corresponds to the extrapolated upper bound on the stopping energy in Ref.17.

While there is considerable sensitivity of the value of $\gamma_{\text{c.m.}}$ for which $L^* > 14$ fm, something striking occurs at $\gamma_{\text{c.m.}} \sim 4$ regardless of the value of α. In addition to showing L^*, Fig. 7 shows the boundaries of the target-chain hadronization regions for the first and last chain in the case that the interactions are time ordered such that $z_i \approx i\lambda$. Curves labeled 1 show the end point

$$z_1(y_{\text{c.m.}}) = \lambda + \frac{m_N}{2\sigma(1+\alpha)} e^{2y_{\text{c.m.}}} \tag{4.27}$$

of hadronization of the first target chain. Curves labeled 2 show the end point of the last target string formed at L^* as given by

$$z_2(y_{\text{c.m.}}) = L^* + \bar{l}(L^*) \ . \tag{4.28}$$

The energy lost by the incident hadron is deposited into the target in the form of secondary particles over a region extending to the larger of curves 1 and 2. For lower energies the hadronization of the last string defines that boundary. For higher energies the first string extends further than the last string. This is simply a consequence of longitudinal growth since the length of the first chain is proportional to the incident laboratory energy while the last chain is proportional to the center-of-mass energy. On the other hand, L^* only grows logarithmically with energy.

When either curve 1 or 2 exceeds the diameter of the nucleus, a fraction of the available energy in the c.m. is lost to secondaries produced outside the nuclei. We define the stopping domain of nuclear collisions as that energy range where not only the baryons come to rest in the c.m. but also where most of secondary particles can be reabsorbed within the Lorentz-contracted nuclear volume. Only if the secondaries resulting from the color-neutralization processes are produced within the nuclear volume can they contribute to heating the high baryon density fireball in the c.m. frame. We see from Fig. 7 that the stopping domain for the heaviest nuclei therefore extends only up to c.m. kinetic energies

$$E_{\text{c.m.}}/A \lesssim 3 \pm 1 \text{ GeV} \ , \tag{4.29}$$

relatively *independent* of the precise value of α.

The total energy deposited within nuclear matter of thickness z is shown in Fig. 8 for the time-ordered case. That energy, $E^{\infty}(z)$, as obtained by integrating Eq. (4.20) up to a given depth z, is shown in units of the energy loss

$$E^*_{\text{stop}} = E_0 - m^* \cosh(y_0/2)$$

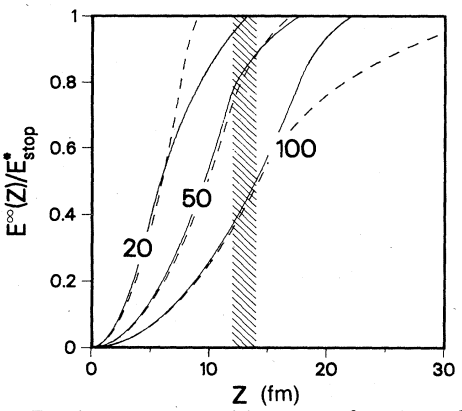

FIG. 8. Total energy deposition as a function of nuclear depth in units of the energy $E^{*}_{\rm stop}=E_0-m^{*}\cosh(y_0/2)$, necessary to reduce the rapidity of an incident proton by one half, i.e., stop the proton in the midrapidity frame. Dashed and solid curves correspond to cases $\alpha=1$ and 3, respectively, and are obtained by integrating dE^{∞}/dz in Fig. 6 from 0 to z. Curves are labeled by incident laboratory energy E_0 in GeV. The stopping domain of nuclear collisions is limited to energies such that the ratio reaches unity before 14 fm.

necessary to stop a baryon in the c.m. system. For a maximum nuclear thickness 12—14 fm, indicated by the shaded region, all the energy loss necessary to reduce the incident rapidity by one half can be deposited within the nuclear volume as long as the incident laboratory energy is below $\sim(20-50)A$ GeV. By $100A$ GeV only $\sim\frac{1}{2}$ of the necessary energy can be deposited within the heaviest nuclei found in nature. Once again note the remarkable insensitivity of these curves to variations of α between 1 and 3.

The relative insensitivity of the stopping domain to dynamical assumptions is a consequence of longitudinal growth. In the case $\alpha=1$ the energy lost forming target chains is twice as large as in the case $\alpha=3$. Therefore, the rapidity of the baryon is reduced in only a fraction of the distance that is necessary in the $\alpha=3$ case. However, the catch is that the hadronization region of target chains extends then twice as far as in the $\alpha=3$ case. Therefore, the stopping domain in the $\alpha=1$ case is limited by the energy at which energetic pions start being produced outside the nuclear volume due to time dilation. On the other hand, in the $\alpha=3$ case the stopping domain is limited by the energy at which the nuclear thickness is no longer sufficient to bring the baryons to rest in the c.m. frame.

The above estimates are only upper bounds because they are based on the assumption, Eq. (4.16), that the chains are produced sequentially. Furthermore, they neglect the effects of fluctuations in the number of chains, their energy fractions, and production points. To study such effects we have written a Monte Carlo program to evaluate the ensemble average in Eq. (4.13) sampling the number of chains from a Poisson, the x_i from the distribution (4.15), and z_i from either (4.16) or (4.17). We have also included the contribution from the projectile chain assuming $z_0=z_1$ in (4.13). Further details of the algorithm and results will be published elsewhere. Here we only quote the final results of such calculations in Table II. In that table the average energy loss and deposition in nuclear matter of thickness 14 fm is given as a function of incident energy E_0. Cases $\alpha=1$ and 3 are again considered. The upper and lower estimates from the energy deposition are obtained using (4.16) or (4.17), respectively. Note that while the energy loss is greater for $\alpha=1$, the energy deposition is smaller in that case because the chains are longer. Note also the saturation of the energy deposition above $E_0>50$ GeV. The most remarkable point is again the relative insensitivity of the total energy deposition to variations in α and the distribution of the z_i. The maximum average energy deposition in 14 fm of nuclear matter is thus $\sim 30\pm 10$ GeV. We also found that the rms fluctuations about the average are fairly large (~ 10 GeV). However, in nuclear collisions those fluctuations are reduced by $A^{-1/3}$.

TABLE II. Average energy loss and deposition (see text). Energies in GeV.

	E_0	30	50	100
$\alpha=3$	$E_{\rm loss}$	24	40	80
	$E_{\rm dep}$	22—26	29—33	38—42
$\alpha=1$	$E_{\rm loss}$	27	47	95
	$E_{\rm dep}$	16—22	20—26	25—31

This Monte Carlo study is therefore consistent with the estimate Eq. (4.29) for the upper bound of the nuclear stopping domain. The error bars quoted in (4.29) therefore correctly reflect the theoretical uncertainties in the present estimates.

Just beyond the stopping domain ($E_{\rm c.m.}/A\gtrsim 3$ GeV) the situation is more uncertain. If $\alpha\sim 1$ is appropriate at those energies, then there could exist a curious intermediate energy region, $3\lesssim E_{\rm c.m}/A<6$ GeV, where baryons would stop on the average in the midrapidity frame but an ever increasing fraction of the energy is lost to fast secondary pions produced outside the Lorentz-contracted nuclear volume. For $\alpha=3$, such an intermediate region would not exist. Experimental information in this energy domain is obviously needed.

We can now estimate the maximum baryon and energy densities that could be reached in the stopping domain. Simple kinematic considerations[31] alone indicate that in the stopping domain the baryon density could reach

$$\rho\sim 2\gamma_{\rm c.m.}\rho_0\sim 8\pm 2\rho_0\,, \tag{4.30}$$

and the energy density could reach

$$\epsilon=\gamma_{\rm c.m.}m_N\rho\sim 5\pm 3\ \text{GeV/fm}^3\,, \tag{4.31}$$

where we input our estimate $\gamma_{\rm c.m.}\lesssim 4$ as the boundary of the stopping domain. In fact, baryon and energy densities up to twice as high could be reached[30] if shock conditions could be reached. On the minus side, not all the secondaries produced in the nuclear volume will be reabsorbed in the fireball due to their finite interaction mean free paths. The leakage of some secondaries would probably compensate for any extra compression beyond the kinematical minimum (4.30). In any case, energy densities in excess of one order of magnitude above the ground-

state value should be easily accessible in central collisions of heavy nuclei at energies $E_{\text{c.m.}} \approx (3\pm1)A$ GeV [$E_{\text{lab}} \sim (17-50)A$ GeV]. The unique feature at these energies is that the baryon density reaches the maximum value that could ever be attained in a laboratory via nuclear collisions.

V. HIGH-ENERGY NUCLEAR COLLISIONS

In this section we make predictions for the nucleon rapidity distributions in the projectile fragmentation region for nuclear collisions beyond the stopping domain. The extension of the multichain model to $B+A \to N+X$, where both B and A are nuclei has been carried out in Ref. 32. With the assumptions in Sec. II, the invariant nucleon inclusive cross section for nuclear collisions can be written as

$$E\frac{d^3\sigma^{BA\to NX}}{dp^3} = \sigma_{BA} g(p_\perp) \frac{dN^{BA}}{dy} , \tag{5.1}$$

where the rapidity density is given by a multiple collision series in analogy to Eq. (2.3) as

$$\frac{dN^{BA}}{dy} = \sum_{m=1}^{B} \sum_{n=1}^{A} P_{BA}(m,n) Q_{m,n}(x) . \tag{5.2}$$

(Charge-exchange and isospin effects will not be considered here.) For a distribution of nuclear-collision impact parameters, $\mathscr{B}(\mathbf{b})$, the probability that m projectile nucleons interact with n target nucleons is given by the usual Glauber expression

$$P_{BA}(m,n) = \int \frac{d^2\mathbf{b}\,\mathscr{B}(\mathbf{b})}{\sigma_{BA}} \int \frac{d^2s}{\sigma_{\text{in}}^{NN}} P_B(m,\mathbf{s}) P_A(n,\mathbf{b}-\mathbf{s}) , \tag{5.3}$$

where $P_B(m,\mathbf{s})$ is the binomial probability that m projectile nucleons interact at relative impact parameter $\mathbf{s}$:

$$P_B(m,\mathbf{s}) = \frac{B!}{m!(B-m)!} [N_B(\mathbf{s})/B]^m [1-N_B(\mathbf{s})/B]^{B-m} . \tag{5.4}$$

Recall that $N_B(\mathbf{s})/B$ with N_B given as in Eq. (2.5) is just the *a priori* probability of finding a projectile nucleon in an infinitely long cylinder of area σ_{in}^{NN} at relative impact parameter $\mathbf{s}$. The product $P_B P_A$ in Eq. (5.3) is then just the probability of finding m projectile and n target nucleons in that same cylinder when the nuclear-collision impact parameter is $\mathbf{b}$. Therefore, $Q_{m,n}$ must be normalized to $m+n$. In Eq. (5.3), σ_{BA} does not correspond to the reaction cross section but rather to a normalization factor ensuring that

$$\sum_{m=1}^{B} \sum_{n=1}^{A} P_{BA}(m,n) = 1 .$$

The Glauber reaction cross section is given by

$$\sigma_r^{BA} = \int d^2\mathbf{b}\,\mathscr{B}(\mathbf{b}) \left[1 - \left[1 - \int \frac{d^2s}{\sigma_{\text{in}}^{NN}} \frac{N_B(\mathbf{s})}{B} \frac{N_A(\mathbf{b}-\mathbf{s})}{A} \right]^{BA} \right] . \tag{5.5}$$

Recall that the inclusive nucleon cross section is normalized as

$$\int d\sigma^{BA\to NX} = \sigma_r^{BA}(B+A) , \tag{5.6}$$

and that it is convenient to decompose $B = W_B + S_B$ and $A = W_A + S_A$, where W_B is the average number of interacting or wounded nucleons and $S_B = B - W_B$ is the average number of noninteracting or spectator nucleons in the projectile nucleus B, and similarly for the target A. From the above relations it is clear that

$$W_B = \int \frac{d^2\mathbf{b}\,\mathscr{B}(\mathbf{b})}{\sigma_r^{BA}} \int \frac{d^2s}{\sigma_{\text{in}}^{NN}} N_B(\mathbf{s}) \times \{1-[1-N_A(\mathbf{b}-\mathbf{s})/A]^A\} , \tag{5.7}$$

with W_A given by interchanging A and B above.

The above relations clearly separate the cumbersome but well-understood geometrical aspects of nuclear collisions from the sought after dynamics specified by the distributions $Q_{m,n}(x)$. It is clear that proton nucleus data[7] provide information only on $Q_{1,n}(x)$ as given by Eq. (2.7). In this paper we explore the consequences of only the simplest assumption—namely, that in the m projectile nucleons fragment independent of one another, i.e.,

$$Q_{m,n}(x) \approx m Q_{1,n}(x) . \tag{5.8}$$

As emphasized in Ref. 22 it is far from obvious that such an independent fragmentation assumption is valid. There is as yet no nuclear collision data to test this assumption. Since such data will be available within a few years (at CERN and BNL), we have calculated the leading-nucleon rapidity density under this assumption using the value of $\alpha = 3$ determined from pA data. The hope is that deviations from our predictions may help uncover possible new phenomena in nuclear collisions. For example, if a locally equilibrated quark-gluon plasma is formed in the fragmentation regions as current speculations suggest,[4,30] then there could be deviations from our predictions.

With Eq. (5.8), the leading-baryon rapidity density is given by

$$\frac{dN^{BA}}{dy} \approx (B-W_B) Q_0(x) + W_B \sum_{n=1}^{A} P_{BA}(n) Q_n(x) , \tag{5.9}$$

where

$$P_{BA}(n) = \int \frac{d^2\mathbf{b}\,\mathscr{B}(\mathbf{b})}{\tilde{\sigma}} \int \frac{d^2s}{\sigma_{\text{in}}^{NN}} \frac{N_B(\mathbf{s})}{B} P_A(n,\mathbf{b}-\mathbf{s}) , \tag{5.10}$$

where σ is chosen to normalize

$$\sum_{n=1}^{A} P_{BA}(n)=1 ,$$

and Q_n is given by Eq. (2.7).

In Fig. 9 our predictions for the leading-baryon rapidity density in central nuclear collisions are shown divided by the atomic number of the beam nucleus. Note that only the projectile fragmentation distributions are shown. According to our assumption on the independence of the target-and projectile-fragmentation regions the target-fragmentation contribution is additive and would substantially modify only the lower half of the rapidity region. We define central collisions via an impact-parameter cut $\mathscr{B}(\mathbf{b})=\theta(2\text{ fm}-b)$. Experimentally, such an impact-parameter range is selected via appropriate associated multiplicity cuts.

The most obvious point to be noted comparing the different reactions is that asymmetric systems such as O + Pb offer a more stringent test of nuclear stopping power than symmetric systems. This is due to the rather large surface contribution with even the heaviest nuclei. A central U + U collision still involves a substantial number of interactions near the surface where only one or two multiple collisions occur. In a central O + Pb collision, on the other hand, every projectile nucleon traverses ~ 12 fm of nuclear matter. Therefore, it is not surprising that O + Pb exhibits the largest rapidity shift of the reactions shown.

From the point of view of new phenomena, deviations from predictions in central U + U collisions could be most interesting. With such large nuclei multiple final-state interactions could lead to local equilibrium and, hopefully, to a high-baryon-density quark-gluon-plasma state in the fragmentation regions. However, our calculations clearly demonstrate that there will always be a substantial source of background due to nuclear halo in collisions of identical nuclei that would contaminate possible signatures of that state. In order to reliably subtract that background, the nuclear-stopping dynamics, via $Q_{m,n}$, must be first understood by extensive studies with light-nuclear beams.

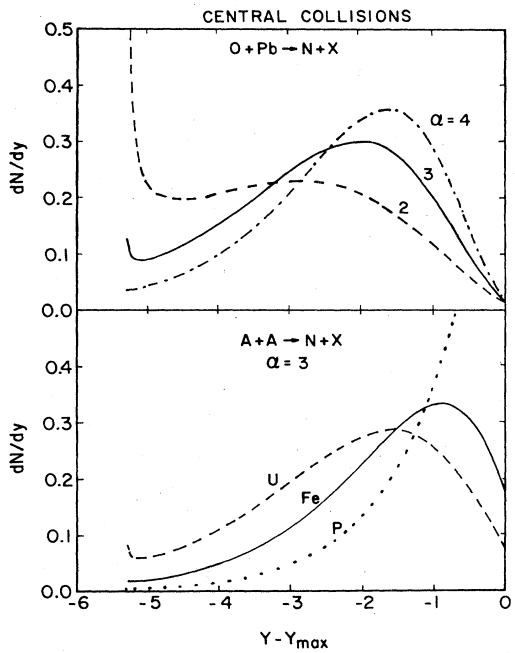

FIG. 9. Predicted nucleon rapidity densities for central nuclear collisions in the projectile frame. Central collisions are defined by integrating impact parameters only up to 2 fm. The rapidity densities are divided by the atomic number of the projectile nucleus. Only the projectile-fragmentation contributions are shown. The dashed, solid, and dashed-dot curves correspond to $\alpha=2$, 3, and 4, respectively.

VI. ADDITIVE QUARK MODEL

We showed in Sec. III that the available data at 100 GeV could be understood in terms of one phenomenological parameter $\alpha\approx 3$ related to the momentum-degradation length via Eq. (4.2). However, we have repeatedly pointed out the limitations of the current phenomenology. In particular, we have stressed that the extrapolated stopping power function in Fig. 3 for nuclear depths >8 fm is not tested by the current data. To help gauge the uncertainties involved, we show in this section that the 100-GeV data can be also understood within the framework of the additive quark model[12,13,15] (AQM). Remarkably, we find that the extrapolation to 14 fm with this model is consistent with the multichain extrapolations. This gives us further confidence in those extrapolations.

In the AQM the incident proton is thought to be composed of three constituent quarks. As the proton passes through a nucleus one, two, or three of those quarks get "wounded" due to interactions. The final observed proton arises from the fragmentation of the wounded projectile. In contrast to the multichain model the fragmentation probability is allowed to depend explicitly on the number of quarks that were wounded in the projectile. In effect the multiple-collision series in Eq. (2.3) is terminated at the term $n=3$. The probabilities $P_A(i)$ are reinterpreted as the probabilities $P_{qA}(i)$ that one, two, or three constituent quarks interact in the nucleus. The Q_n are regarded as unknown fragmentation functions to be determined by fitting data.

The probability that i projectile constituent quarks are wounded is given in analogy to Eq. (2.4) by

$$P_{qA}(i)=\int \frac{d^2\mathbf{b}}{\sigma_{\text{in}}^{pA}} \frac{3!}{i!(3-i)!} p_{qA}(\mathbf{b})^i[1-p_{qA}(\mathbf{b})]^{3-i} , \tag{6.1}$$

where $p_{qA}(\mathbf{b})$ is the probability that a constituent quark interacts at impact parameter $\mathbf{b}$,

$$p_{qA}(\mathbf{b})=1-\left[1-\sigma_{qN}\int dz\,\rho_A(z,\mathbf{b})/A\right]^A \approx 1-e^{-\sigma_{qN}N_A(\mathbf{b})/\sigma_{NN}} , \tag{6.2}$$

and the reaction cross section is given by

$$\sigma_{\text{in}}^{pA}=\int d^2\mathbf{b}\{1-[1-p_{qA}(\mathbf{b})]^3\} . \tag{6.3}$$

In the spirit of that model we take the constituent quark-nucleon cross section to be $\sigma_{qN}=10$ mb. The probabilities for wounding quarks are shown in Fig. 10 as a function of

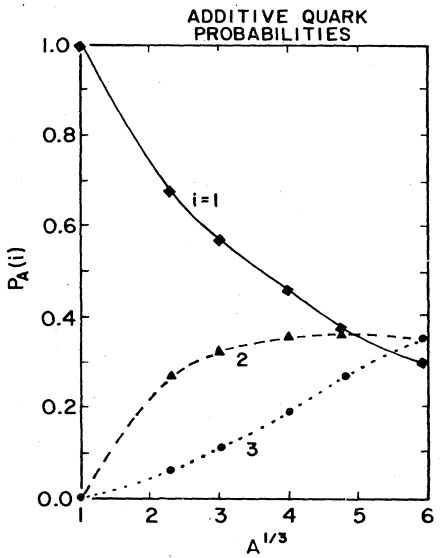

FIG. 10. Additive quark probabilities for wounding 1, 2, or 3 constituent quarks with effective cross section $\sigma_{qN}=10$ mb on Wood-Saxon nuclei (Ref. 33).

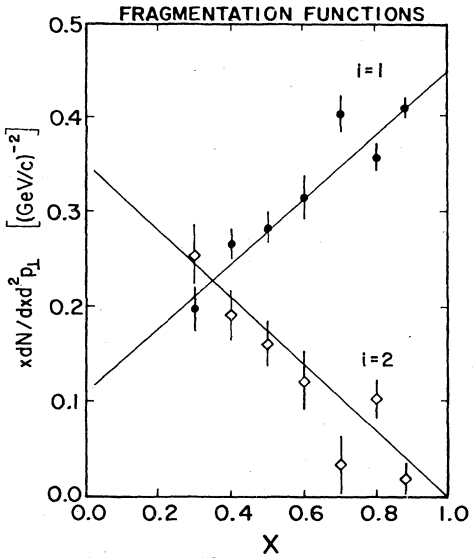

FIG. 11. Invariant proton fragmentation distributions in the additive quark model (Refs. 13 and 15) resulting from wounding one (solid dot) or two (open circle) quarks as determined by a χ^2 fit to data (Ref. 7). Wounding of all three quarks is assumed to lead to negligible proton production in the measured kinematic range. The data points are obtained by a χ^2 fit to the $pA\to pX$ data (Ref. 7) and lines correspond to linear fits.

$A^{1/3}$. For these calculations we used the Wood-Saxon parameters of Ref. 33. Use of the parameters in Eqs. (3.3) and (3.4) lead to the same probabilities within 10%. This is the order of magnitude uncertainty in the choice of σ_{qN} in any case. Note how large is the probability that only one constituent quark interacts even for Pb. Note further that we have set $P_{qN}(i)=\delta_{i,1}$ as in Refs. 13 and 15 although a strict application of Eq. (6.1) to $A=1$ would yield $P_{qN}(1)\approx 0.8$–0.9. This is an additional model assumption that is necessary in order to fit the A dependence of the data form $A=1$ to $A=208$. With this assumption $Q_1(x)$ should correspond to the $p+p\to p+X$ distribution. In fact, we did not constrain Q_1 to equal the proton target data, but rather we determined the Q_i at each value of x by a minimum χ^2 fit to all six ($A=p$,C,Al,Cu,Ag,Pb) reactions. Such a method was used in Refs. 13 and 15 to fit Λ^0 inclusive data.

With a three-parameter fit to six data points at each value of x we found obviously a very shallow χ^2 minimum with enormous uncertainties and correlations among the Q_i. However, the results suggested that in the measured x range, the contribution to dN/dy from collisions involving three wounded quarks could be neglected. Therefore, we tried a fit constraining $Q_3=0$ as in Refs. 13 and 15. The invariant proton distributions, $x\,d^3N_i/dx\,d^2p_\perp$, for $i=1$ (solid dots) and $i=2$ (open circles) as determined from such a fit are shown in Fig. 11. The solid lines represent linear least square fits to those distributions. We find that we can parametrize those invariant distributions for $x>0.3$ and $p_\perp=0.3$ GeV/c in $(\mathrm{GeV}/c)^{-2}$ units by

$$\begin{aligned} x\,d^3N_1/dx\,d^2p_\perp &\approx 0.11+0.34x\ , \\ x\,d^3N_2/dx\,d^2p_\perp &\approx 0.35(1-x)\ , \\ x\,d^3N_3/dx\,d^2p_\perp &\approx 0\ . \end{aligned} \tag{6.4}$$

With the above fragmentation functions the invariant proton inclusive cross section in the AQM is

$$E\frac{d^3\sigma^{pA\to pX}}{dp^3}=x\sigma_{\mathrm{in}}^{pA}\left[P_A(1)\frac{d^3N_1}{dx\,d^2p_\perp}+P_A(2)\frac{d^3N_2}{dx\,d^2p_\perp}\right]. \tag{6.5}$$

In Fig. 12 the solid curves calculated from the above relation are compared to the Busza data.[7] We find that the AQM can reproduce the data as well as the multichain model. Of course, there is a much larger degree of freedom in the AQM through three arbitrary fragmentation functions.

For purposes of this paper the important question is what this fit implies about nuclear stopping power. Unfortunately, the data only go down to $x=0.3$, and the model provides no clues of how to extrapolate the fragmentation functions to low x. Thus, strictly speaking, the nuclear stopping power remains undetermined from the available data. We can, nevertheless, try to estimate it in the spirit of Ref. 17 by extrapolating Eq. (6.4) to a lower cutoff x_c. We took $x_c=0.073$, corresponding to an extrapolation to midrapidity. With this extrapolation we found that the average momentum fraction carried by the leading proton is $x_1\approx 0.45$ and $x_2\approx 0.25$ if one or two quarks are wounded, respectively. With a form of Q_3 compatible with it being negligible for $x>0.3$, the leading proton would carry only a fraction $x_3\lesssim 0.15$ of the incident energy if all three quarks were wounded. These results are therefore compatible with

$$x_i\approx(\tfrac{1}{2})^i\ . \tag{6.6}$$

With Eq. (6.6) the average momentum fraction carried by

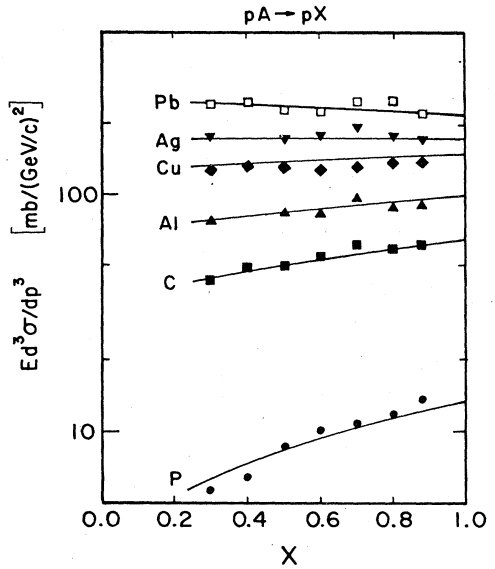

FIG. 12. Comparison of proton inclusive data (Ref. 7) with calculations using the AQM fragmentation functions of Fig. 11 as parametrized by Eq. (6.4).

the leading proton after traversing a thickness z of nuclear matter is

$$\langle x \rangle_z \approx \tfrac{1}{8}(1+e^{-z/\lambda_q})^3 , \tag{6.7}$$

where $\lambda_q \approx 7$ fm is the mean free path of a constituent quark in nuclear matter. For $x=14$ fm, Eq. (6.7) gives $\langle x \rangle \approx 0.18$. In comparison, the multichain model extrapolation via Eq. (2.32) to 14 fm gives $\langle x \rangle \approx 0.19$ for a nucleon inelastic mean free path $\lambda = 2.08$ fm. It is remarkable how stable is this extrapolation to major changes in the model assumptions as long as the 100-GeV data are used to constrain the parameters of the models. For comparison, the incoherent cascade model, which fails to reproduce the data, would give $\langle x \rangle \approx 0.03$.

VII. CONCLUDING REMARKS

The main purpose of this paper was to extract as much information on nuclear stopping power as possible from the limited data[7] on $p+A \to p+X$ at 100 GeV. Making several strong assumptions concerning transverse factorization and scaling dynamics, we applied the multichain model[9] to extract one physical parameter, $\alpha = 3 \pm 1$, by fitting the invariant cross sections for $A = p$, C, Al, Cu, Ag, and Pb at $p_\perp = 0.3$ GeV/c and $x > 0.3$. This parameter was shown to be related to the momentum-degradation length, $\Lambda_p = 8 \pm 2$ fm, that controls the exponential decrease of the final baryon energy fraction as a function of nuclear thickness. We pointed out, however, that the phenomenon of longitudinal growth[2] implies that energy loss via multiparticle production occurs over an ever increasing length scale proportional to the energy. By analyzing the space-time development of particle production in the multichain model we were led to conclude that there are in fact multiple length scales associated with the hadronization scales of the different target chains created during the collision. This follows because hadron-nucleus collisions involve several independent processes due to the composite nature of hadrons: each subprocess involving only a fraction of the incident energy. The longest of those chains was found to be on the average $1/(1+\alpha)$ smaller than the naive longitudinal length scale[2-4] given by E_0/σ.

The second purpose of this paper was to apply the empirical stopping power to determine an upper bound on the stopping domain in nuclear collisions. In this paper we define the stopping domain to be that energy range in which collisions of slabs of nuclear thickness 14 fm lead not only to the stopping of most baryons in the center-of-mass system but also to the production of most of the energetic secondaries within the Lorentz-contracted nuclear volume ($14/\gamma_{\text{c.m.}}$). For this we had to extrapolate to lower energies and greater nuclear depths than covered by the current data. We found in Sec. III D that we should expect violations from the simple scaling hypothesis, but that those violations tend to increase the stopping power of nuclei at lower energies. Unfortunately, there is insufficient data at present to determine the precise form of the energy dependence of those violations. Therefore, in estimating the boundary of the stopping domain in nuclear collisions we varied the parameter of our model from $\alpha = 1$ to 3 to cover the large uncertainties associated with scaling violations. We found, however, that because of longitudinal growth the bound on the stopping domain, $E_{\text{c.m.}} \lesssim (3 \pm 1)A$ GeV, was relatively independent of the value of α. We showed further that the extrapolation to nuclear depths ~ 14 fm was stable against variations of the model assumptions by considering limitations on the number of target chains and by varying the assumptions on projectile fragmentations via the additive quark model.[12,13,15] This gave us further confidence about our estimate of $E^{\max}_{\text{c.m.}}$. A Monte Carlo study also showed that within the errors quoted, the maximum stopping energy does not depend sensitively on the unknown distribution of the interaction points.

Beyond the maximum energy for stopping the situation is less clear. Eventually, at very high energies $E_{\text{c.m.}} \gtrsim 100A$ GeV the fragmentation regions and central region separate although the nuclei shatter over several units of rapidity. The energy range above the stopping domain $\sim (3-5)A$ GeV is most likely characterized by large fluctuations. Some collisions may accidently lead to complete stopping, while others only to shattering. In this region the notion of an average collision may not be useful. The stopping domain has the advantage that the maximum baryon and energy densities are more or less fixed by kinematics. With maximum stopping energies $E_{\text{c.m.}}/A$ on the order of a few GeV, our analysis is consistent with previous expectations[16-18] that baryon densities and energy densities on the order of 10 times those found in ground-state nuclei could indeed be achieved in central collisions of heavy nuclei. Whether that energy density is enough to reach the quark-gluon-plasma phase remains an exciting open question.

Finally, there is a clear need for more extensive data to help resolve some of the many remaining uncertainties associated with nuclear stopping power. Systematic mea-

surements as a function of energy in the range 20 to 400 GeV are important to map out the scaling violations. Also important are measurements of inclusive cross sections with associated multiplicity triggers to probe stopping power to greater depths $z \sim 14$ fm. Finally, central collision studies with light nuclear beams are necessary to test linear extrapolations from pA reactions and look for possible nonlinear effect. We have made predictions for central nuclear collisions to establish a baseline in looking for novel effects.

ACKNOWLEDGMENTS

Discussions with W. Busza, L. P. Csernai, A. Goldhaber, W. Swiatecki, and C. Y. Wong have been particularly useful. One of us (H.S.) acknowledges support by the Faculty of Engineering, Seikei University under the Grant of Special Research Project 1984. Another of us (M.G.) is grateful to the Ministry of Education of Japan for support as visiting professor at the Institute of Nuclear Study from March to June 1984 and acknowledges support by the Director, Office of Energy Research, Division of Nuclear Physics of the Office of High Energy and Nuclear Physics of the U.S. Department of Energy under Contract No. DE-AC03-76SF00098.

*Permanent address: Nuclear Science Division, Mailstop 70A-3307, Lawrence Berkeley Laboratory, Berkeley, CA 94720.

[1]K. Gottfried, in *High Energy Physics and Nuclear Structure, Proceedings of the Fifth International Conference, Uppsala, Sweden, 1973,* edited by G. Tibell (North-Holland, Amsterdam/American Elsevier, New York, 1974), p. 79.

[2]O. V. Kancheli, Pis'ma Zh. Eksp. Teor. Fiz. **18**, 465 (1973) [JETP Lett. **18**, 274 (1973)]; N. N. Nikolaev, Fiz. Elem. Chastits At. Yadra **12**, 162 (1981) [Sov. J. Part. Nucl. **12**, 63 (1981)].

[3]J. D. Bjorken, in *Current Induced Reactions,* proceedings of the International Summer Institute on Theoretical Particle Physics, Hamburg, 1975, edited by S. G. Körner, G. Kramer, and D. Scholdkneckt (Lecture Notes in Physics, Vol. 56) (Springer, Berlin, 1976), p. 73.

[4]R.Annishetty, P. Koehler, and L. McLerran, Phys. Rev. D **22**, 2793 (1980).

[5]S. Hirabayashi, K. Kobayakawa, and T. Morii, Prog. Theor. Phys. **61**, 117 (1979).

[6]W. Busza *et al.*, Phys. Rev. Lett. **34**, 836 (1975); C. Halliwell *et al., ibid.* **39**, 1499 (1977); J. E. Elias *et al.*, Phys. Rev. D **22**, 13 (1980); C. De Marzo *et al., ibid.* **29**, 2476 (1984).

[7]A. Barton, *et al.*, Phys. Rev. D **27**, 2580 (1983).

[8]A. Capella and A. Krzywicki, Phys. Lett. **67B**, 84 (1977).

[9]K. Kinoshita, A. Minaka, and H. Sumiyoshi, Prog. Theor. Phys. **63**, 928 (1980).

[10]H. Sumiyoshi and M. Uehara, in *Proceedings of the Meeting on Recent Progress in Production Mechanisms in High Energy Collisions of Nucleons and Nuclei, Kyoto, 1981* (RIFP, Kyoto University, 1981), p. 63.

[11]A. Capella and J. Tran Thanh Van, Z. Phys. C **10**, 249 (1981).

[12]V. V. Anisovich, Yu. M. Shbelsky, and V. M. Shekhter, Nucl. Phys. **B133**, 477 (1978).

[13]A. Białas and E. Białas, Phys. Rev. D **20**, 2854 (1979).

[14]A. Białas and W. Czyz, Nucl. Phys. **B194**, 21 (1982).

[15]F. Takagi, Prog. Theor. Phys. **65**, 1350 (1981); Phys. Rev. D **27**, 1461 (1983).

[16]*Quark Matter '83,* Proceedings of the Third International Conference on Ultrarelativistic Nucleus-Nucleus Collisions, edited by T. W. Ludlam and H. E. Wegner [Nucl. Phys. **A418**, (1984)].

[17]W. Busza and A. S. Goldhaber, Phys. Lett. **139B**, 235 (1984).

[18]M. Gyulassy, in *Multiparticle Dynamics, 1983,* proceedings of the XIV International Symposium, Lake Tahoe, edited by P. Yager and J. F. Gunion (World Scientific, Singapore, 1984), p. 1008; in *Proceedings of the 6th Balaton Conference on Nuclear Physics, 1983,* edited by J. Ero (KFKI Institute, Budapest, 1983), p. 489.

[19]R. C. Hwa, Phys. Rev. Lett. **52**, 492 (1984).

[20]L. P. Csernai and J. Kapusta, Phys. Rev. **D29**, 2664 (1984); **31**, 2795 (1985).

[21]C. Y. Wong, Phys. Rev. Lett. **52**, 1393 (1984); Phys. Rev. D **30**, 961 (1984); **30**, 972 (1984).

[22]J. Hufner and A. Klar, Phys. Lett. **145B**, 167 (1984).

[23]S. J. Brodsky, J. F. Gunion, and J. H. Kuhn, Phys. Rev. Lett. **39**, 1120 (1977).

[24]R. J. Glauber, in *Lectures in Theoretical Physics,* edited by W. E. Brittin and L. G. Dunham (Interscience, New York, 1959), Vol. 1, p. 315.

[25]H. Sato (private communication).

[26]S. A. Carrol *et al.*, Phys. Lett. **80B**, 319 (1979).

[27]T. Eichten *et al.*, Nucl. Phys. **B44**, 333 (1972).

[28]V. Blobel *et al.*, Nucl. Phys. **B69**, 454 (1974).

[29]L. P. Remsberg, in *Proceedings of the 7th High Energy Heavy Ion Study, Darmstadt, 1984,* edited by R. Bock, H. H. Gutbrod, and R. Stock (Gesellschaft für Shwerionforschung, Darmstadt Report No. GSI-85-10), p. 439.

[30]M. Gyulassy, in *Quark Matter Formation and Heavy Ion Collisions,* proceedings of the Bielefeld Workshop, 1982, edited by M. Jacob and H. Satz (World Scientific, Singapore, 1982), p. 81.

[31]A. S. Goldhaber, Nature **275**, 114 (1978).

[32]K. Kinoshita, A. Minaka, and H. Sumiyoshi, Z. Phys. C **8**, 205 (1981).

[33]E. Franco *et al.*, Phys. Rev. C **6**, 748 (1972).